THESIS FOR THE DEGREE OF LICENTIATE OF ENGINEERING

In-situ Investigations of Lithium-Sulfur Batteries

Matthew J. Sadd

Department of Physics

CHALMERS UNIVERSITY OF TECHNOLOGY

Gothenburg, Sweden 2019

In-situ Investigations of Lithium-Sulfur Batteries

MATTHEW J. SADD

Department of Physics
Chalmers University of Technology
SE-412 96 Gothenburg
Sweden
Telephone + 46 (0)31-772 1000

Printed by Chalmers Reproservice
Gothenburg, Sweden 2019

Abstract

As the demand for high energy-density storage devices increases, we must look beyond the current state of the art technology, the lithium-ion battery. Lithium-ion battery technologies are approaching their theoretical limit in terms of capacity, and now that the demand for longer-range electric vehicles (EVs) and the implementation of grid storage is increasing, we need to provide technologies that can go beyond what is currently possible. In order to increase the capacity of batteries, and to develop more sustainable technologies to meet the rising demand, we must turn to new chemistries.

A suggested Next-Generation Battery chemistry is based on the electrochemical reaction between lithium and sulfur. This chemistry does not rely on intercalation reactions as the Li-ion battery is, but instead employs conversion chemistry. At discharge elemental sulfur is reduced and converted to polysulfides, yielding a maximum specific capacity of 1672 $mAhg^{-1}$, up to 6 times the theoretical maximum capacity of state-of-the-art Li-ion battery materials. Thus, the lithium-sulfur technology is a suitable successor due to a potentially higher energy density. In addition, there is also the potential to create sustainable systems made from low-cost and high abundance elements, while also creating less toxic and safer devices than those which are currently available for commercially.

In our quest to reach a working lithium-sulfur battery there are a series of challenges that must be addressed, many of which originate from the complex reactions and mechanisms of the lithium-sulfur cell. Soluble Li-polysulfide species are formed during cell operation in commonly used electrolytes, these species are highly mobile and react with the Li-metal anode used. This interaction leads to the unwanted reduction of polysulfide species at the anode, causing the polysulfide shuttle, and capacity fade due to the irreversible deposition of active material on the Li-metal surface.

A series of methods have been used to address the unwanted reactions, such as the use of novel additives in the electrolyte to form a stable solid-electrolyte interphase (SEI). In this thesis the unique character of polysulfide species is addressed, and methods discussed will show how control of polysulfide dissolution and speciation can be used to improve cell performance. This improvement is realised by designing new electrolytes that block the passage of polysulfides to the Li-metal anode's surface, and by using polysulfide species in the electrolyte to enable longer lifetime cells by preventing sulfur dissolution while simultaneously supplementing the energy density of a cell by acting as a Li-salt. However, the mechanism of how the polysulfide species behave is not fully understood. To monitor how polysulfides interact with the Li-metal when they act as charge carriers, *operando* Raman spectroscopy has been employed to track polysulfide concentration changes in a cell and reveal new insights on the mechanisms of polysulfides as Li-salts.

List of Papers

I Designing a Safe Electrolyte Enabling Long-Life Li/S Batteries

M. Agostini, M. Sadd, S. Xiong, C. Cavallo, J. Heo, J. H. Ahn, and A. Matic
ChemSusChem 2019, 12, 1–10. https://doi.org/10.1002/cssc.201901770

II Rational Design of Low Cost and High Energy Lithium Batteries through Tailored Fluorine-Free Electrolyte and Nanostructured S/C Composite

M. Agostini, D. -H. Lim, M.Sadd, J. -Y. Hang, S. Brutti, J. W. Heo, J. H. Ahn, Y. K. Sun, and A. Matic
ChemSusChem 2018, 11, 2981–2986. https://doi.org/10.1002/cssc.201801017

III Polysulfide Migration and Conversion in Lithium-Sulfur cells

M. Sadd, M. Agostini, P. Jankowski, S. Xiong, W. Lei, J. Song, A. Matic.
Manuscript

Contribution Report

I Designing a Safe Electrolyte Enabling Long-Life Li/S batteries

- Prepared electrolytes, performed Raman analysis, assisted with; conductivity, viscosity, electrochemical analysis, discussion and preparation of the manuscript. I authored the section on Raman analysis.

II Rational Design of Low Cost and High Energy Lithium Batteries through Tailored Fluorine-free Electrolyte and Nanostructured S/C Composite

- Assisted with electrochemical analysis, discussion and writing of the manuscript.

III Polysulfide Migration and Conversion in Catholyte Lithium-Sulfur Cells

- Prepared all materials, performed Raman analysis, performed all electrochemical analysis, discussed results with co-authors, and wrote the manuscript.

Table of Contents

1 Introduction

The world today surrounds us with electronic devices that require some form electrical energy storage, from the mobile phones that have become commonplace in our day to day lives to electric cars which are ever-growing in popularity, and from automated external defibrillators that we keep in our public spaces which save lives to pacemakers which keep hearts beating. There is a plethora of examples of devices and systems which require the use of electrical energy storage.

Electrochemical energy storage includes super-capacitors, and most notably, batteries. The most well-known example of batteries is the Lithium-ion battery (Li-ion). The Li-ion battery can be found in mobile phones, laptops and now in vehicles as we look towards electrifying the transport sector. The Li-ion battery itself has been in use since 1991 when it was first commercialised by Sony, making it a technology that is over a quarter of a century old. Research on the Li-ion battery can be traced back as far as the 60s, with research on the commonly used Lithium Cobalt Oxide cell being performed in 1980.[1] However, there is still intense research going on as new applications demand improvements in performance, such as improved rate capacity, longer lifetimes, and higher voltages.

Batteries are starting to show that they play a vital role in the fight to tackle climate change and global CO_2 emissions. It has been identified that the major sources of CO_2 emissions are from the electricity and heat production, and transport sectors,[2] as seen in Figure 1.

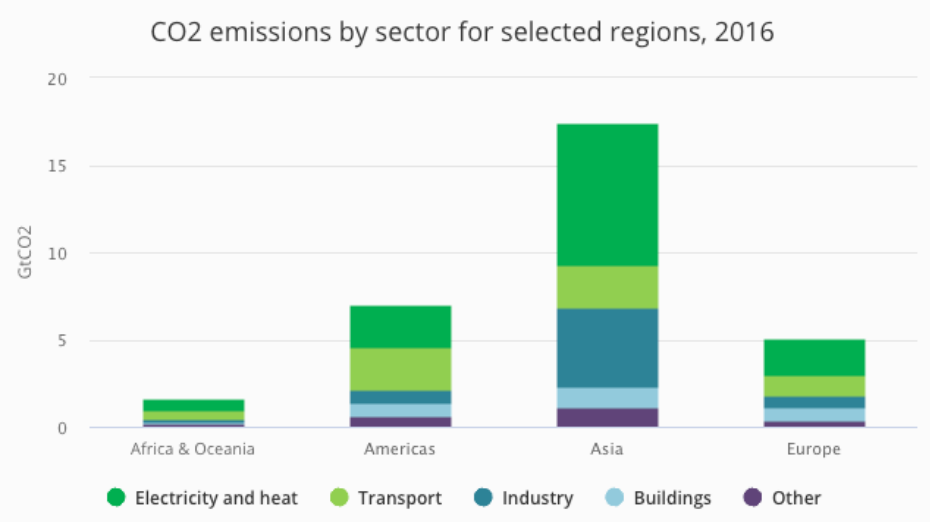

Figure 1 Graph of CO2 emissions by sector, taken from the International Energy Agency.[3]

Even though it is not a total and complete solution, a transition to electric vehicles can aid the effort to reduce CO_2 emissions, with our petrol and diesel combustion engine vehicles being replaced by hybrid electric and all-electric vehicles. In addition to the Li-ion battery's ever-increasing prevalence due to its demand in the electric vehicle market, there is also a secondary demand for high energy-density storage in the fight to tackle CO_2 emissions, that is the implementation of large-scale and micro-grid storage.

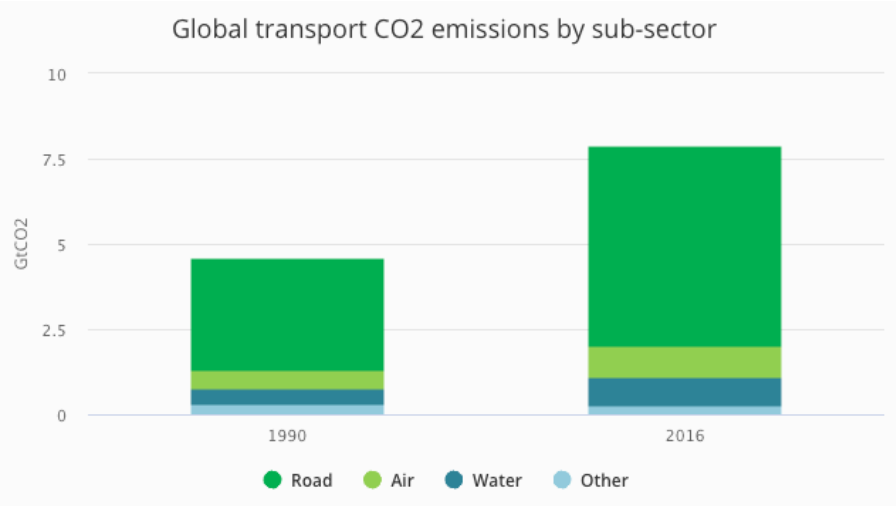

Figure 2 Graph of CO2 emissions in the transport sector, taken from the International Energy Agency.[3]

Grid storage can typically rely on a battery technology that does not have a high energy density since the application of it is stationary, the main requirement would be for the battery technology to be cost-effective and sustainable. Similarly, in order to favour a shift from CEVs to EVs, cost and sustainability are major obstacles that need to be overcome. A reduction in the cost of the vehicle would be related to cheaper batteries, currently, EVs cost significantly more than their CEV counterpart.[4] In addition, we also need to see an increase in the driving range of the EV, with the range being related to the energy density of the battery being used. From Figure 2, it can be seen that road vehicles are major contributors to CO_2 emissions; however, the seconds biggest source of transport emissions comes from aircrafts. The electrification of planes has already begun, with a joint effort from Airbus, Siemens and Rolls-Royce to create a hybrid-electric plane.[5] Moving forward, to see the electrification of planes, a high energy density battery needs to be developed that can provide both range and weight benefits to the air travel sector. A report by *Schäfer et al.* suggested that if we are able to develop battery packs that have an energy density of 800 Wh/kg, this could then enable fully electric flight exceeding 1000 km in range.[6]

The aim of the work presented in this thesis is to investigate mechanisms behind the performance of the lithium-sulfur system, a Next Generation battery that has a higher theoretical specific capacity compared to current state of the art technologies. Through our investigations, the unique behaviour of soluble polysulfide species which are formed during operation, is explored. Methods to stabilise the performance of the anode are explored by investigating a novel electrolyte that blocks the interactions of Li-metal and polysulfide species, enabling longer cycle life. Cells with longer cycle lives are further explored by employing polysulfide species as sulfur dissolution buffers, however in this same system, polysulfide species act as charge carriers and increase the energy density of the cell to values that surpass what Li-ion batteries are currently capable of. However, the unique mechanism of how the polysulfide species behave when they act as the Li-salt is not fully understood. To monitor this behaviour, *operando* Raman spectroscopy has been employed to track polysulfide concentration changes and reveal new insights on their interactions with the Li-metal anode.

2 Batteries

When we say the term ‘battery’ today, we commonly refer to an electrical energy storage device, which specifically is a set of connected galvanic cells. A galvanic cell refers to a single electrochemical cell which, in the case of batteries, typically contains an anode, a cathode, current collectors, an electrically insulating separator and an electrolyte. Batteries can be classified in two types of cell; a primary cell that will discharge once[7] due to the irreversible nature of the chemical reaction that has occurred, and a secondary cell that can be recharged[7] due to reversible chemical reactions.

The most well-known secondary cell technology today is the Li-ion cell. Li-ion is an umbrella term that represents a multitude of cathode chemistries such as $LiFePO_4$, $LiMn_2O_2$, and $LiCoO_2$, just to name a few, often coupled with a graphite anode. All these chemistries carry various unique characteristics, considering cyclability, capacity, operating voltage, and safety, however they all rely on intercalation processes, where Li^+ ions are inserted into free sites in a host structure. In the case of the $LiCoO_2$ and graphite (C_6) the following reversible reaction occurs:

$$LiCoO_2 + C_6 \rightleftharpoons LiC_6 + CoO_2$$

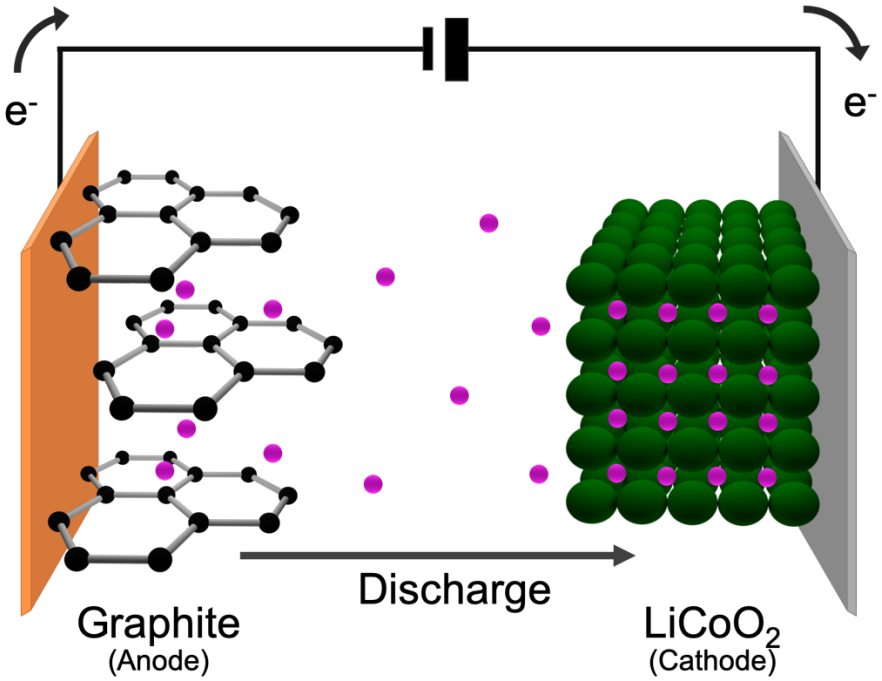

Figure 3 Schematic of electrodes and the movement of Li^+ ions inside a Li-ion cell.

In a galvanic cell there are spontaneous oxidation (loss of an electron) and reduction (gain of an electron) reactions that occur at the electrodes that provide a flow of electrons:

Reduction: $$O^+ + ne^- \rightleftharpoons R$$ Equation 1

Oxidation: $$R \rightleftharpoons O^+ + ne^-$$ Equation 2

These processes, along with the concentrations of the species in a cell, provide the potential of an electrode, and gives the cell its voltage (potential difference). The potential of an electrode, based on its redox reaction, is described by the Nernst equation, where the potential is derived from the Gibb's energy of a system:[8]

$$\Delta G = -nFE$$

$$\Delta G^\circ = -nFE^\circ$$

$$\Delta G = \Delta G^\circ + RT \ln Q$$

$$-nFE = -nFE^\circ + RT \ln Q$$

$$E = E^\circ + \frac{2.3RT}{nF} \log \frac{[\mathrm{O}]}{[\mathrm{R}]}$$ Equation 3

Here, E_e is the equilibrium potential of a redox couple in solution, E_e° is the standard potential of the couple in solution, R ideal gas constant, T temperature, F Faraday constant, n the number of electrons transferred, and finally [O] and [R] are the concentrations of the oxidised and reduced species, respectively, which are related to their chemical activity. In batteries we very seldom deal with a system where the oxidant and reactant are dissolved in solution, instead we commonly have have a system where the oxidant and reductant have a minimal concentration in solution when compared to the concentration of the electrolyte. Thus their activities (concentrations) are similar, often cancelling each other out. Additionally, the activity of a metal is 1 and activity of an element at a pressure of one atmosphere is also 1.[8]

However if we have the following reaction, then the Nernst equation becomes:

$$M^{n+} + ne^- \rightleftharpoons M$$ Equation 4

$$E_e = E_e^\circ + \frac{2.3RT}{nF} \log \left(c_{M^{n+}}\right)$$ Equation 5

These equation determines the potential of our electrodes and hence the potential difference, the cell voltage.

The Nernst equation describes the voltage a single electrode but does not explain the mechanism that underpins where the voltage and electron flow originate from. Figure 4 shows the underlying processes of mass transport and electron transfer, necessary processes that occur at the electrodes to support the oxidation and reduction.

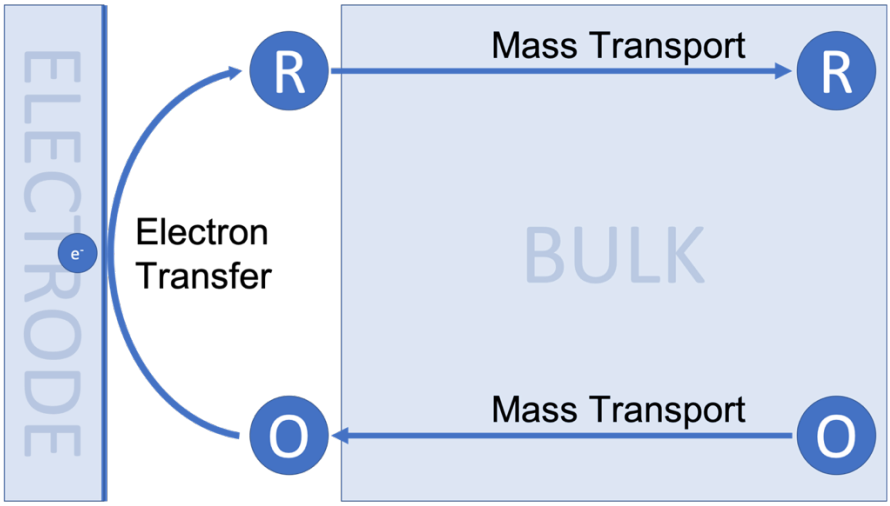

Figure 4 Mass transport and electron transfer at a single electrode.

During discharge, oxidation takes place at the anode and reduction takes place at the cathode. For a given species in the cell to be oxidised, or reduced, it needs to travel from the 'bulk' of the electrolyte, to the electrode surface. This process is known as mass transport, and the mechanism that allows this movement is either diffusion along a diffusion gradient or the migration of a charged species through an electric field. We also see from Figure 4, that there 3 discrete processes occurring during the reduction, or oxidation of our species, and the slowest of these processes is what will determine the kinetics of the oxidation/reduction process.[8] Once a species reaches the electrode surface electron transfer can occur, in the case of reduction, the species (O) will come into contact with the electrode surface and gain an electron (ne^-) resulting in the species being reduced (R) as shown in Equation 1.

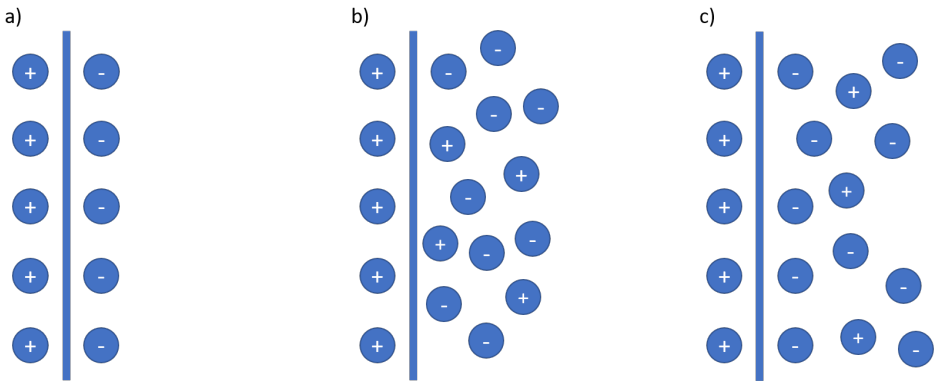

Figure 5 Models of the electric double layer. a) Helmholtz model, b) Gouy-Chapman model, c) Stern model.[8,9]

When looking at the process of reduction and oxidation at the electrode surface, the presence of an electric double layer plays an important role when considering the dynamics at the electrode. Over time there have been various models used to describe the electric double layer at an electrode's surface. Initially, the Helmholtz model[9] suggested that a single layer of ions accumulates at the electrode surface to balance the charge of the electrode. However, this model did not accommodate the free movement of ions through an electrolyte. In the Gouy-Chapman model,[9] ions are free to move, in this case there would be a high concentration of ions close to the electrode surface and would gradually drop of with distance from the electrode, known as the diffuse layer. A final iteration, the Stern model,[9] showed there would be a layer of ions at the electrode surface combined with a diffuse layer.

The models show that as we polarise the electrode with a potential, whether that be positive or negative, ions in the electrolyte will counter the charge of the electrode, this has one of two functions. The first is that it will draw charged species to its surface, often salt present in the electrolyte, and the second is that it then can confine these salts at the electrode surface. In the case of conversion chemistry, this can potentially hinder the ability of the electrode to convert species reaching the electrode surface. In addition, the electric double layer affects the kinetics of the electrode and in turn the speed at which we can discharge or charge the cell.

The rate at which we discharge or charge a cell is commonly referred to as the C-rate. It represents the current applied to the cell and hence the time it will take for full discharge or charge, with respect to the theoretical specific capacity of the cell. For instance, for a cell with a theoretical specific capacity of $275mAhg^{-1}$, we would have the following values for C-rate for different applied specific currents:

C-rate (C)	Applied Current (mAg^{-1})	Time to discharge (h)
0.1	27.5	10
1	275	1
10	2750	0.1

2.1 Lithium Batteries

The current state of the art battery technology is the Li-ion battery, when looking at the periodic table we see why the use of lithium as a charge carrier is favourable for batteries. It sits in the first period of the second row, it is the 3rd element of the table and has a molecular weight of 6.94 $gmol^{-1}$. It is light, and it is highly reactive, giving it a low potential, -3.04 V, vs. the standard hydrogen electrode. However, the use of metallic lithium holds challenges of dendrite formation, and a graphite anode instead used in commercial Li-ion batteries.

The theoretical specific capacity for Li-ion ($LiCoO_2$) batteries, representing the theoretical number of electrons transferred for a specified active material, for a $LiCoO_2$ battery the value is 275 $mAhg^{-1}$.[7] For this same battery the theoretical energy density, which equates to the amount of useful work that can be done, is 410 $Whkg^{-1}$ based on the capacities of the anode and cathode active material and a nominal cell voltage, although practically energy densities of 150 $Whkg^{-1}$ are achieved.[7,10]

Cathode	During discharge this is where the process of reduction occurs, in a Li-ion battery the cathode material is a layered oxide and in the case of $LiCoO_2$ the following reaction occurs to accept an electron: $$Li^+ + e^- + CoO_2 \rightleftharpoons LiCoO_2$$ This reaction carries the theoretical specific capacity of 275 $mAhg^{-1}$.
Anode	During discharge this is where the process of oxidation occurs, in a Li-ion battery the anode material is made of graphite (C_6) and results in the following reaction to produce an electron: $$LiC_6 \rightleftharpoons Li^+ + e^- + C_6$$ This reaction carries the theoretical specific capacity of 372 $mAhg^{-1}$.
Electrolyte	It is made up of a solvent, or solvents, and a salt. In the case of lithium-ion batteries, an example of the solvents used are Dimethyl Carbonate (DMC) and Ethylene Carbonate (EC), with the salt being Lithium Hexafluorophosphate ($LiPF_6$).
Other	Other components include the current collectors that both the anode and cathode must be supported by, and the separator which holds the electrolyte while being a physical barrier which prevents electric short circuits.

Even though the Li-ion battery is the current state-of-the-art technology in use today, there are several disadvantages to its use in EVs and for grid storage. The first issue is cost, and the battery is often the cost limiting factor in EVs and contributes to the high price of the vehicle. The second issue is that we are reaching a point where we are unable to push additional capacity out of the cathode material and the energy density is limited by the cathode capacity.

A final issue with Li-ion cells, their safety. There is potential for Li-ion cells to suffer from thermal runaway of the oxide material, short-circuit of the electrodes, combining this with the flammability of the solvents in electrolyte poses a serious risk of cell combustion.

2.2 Next-Generation Batteries

To move beyond the limitations of the Li-ion battery there are several chemistries that have been proposed, typically referred to as Next-Generation Batteries, summarised in **Error! Reference source not found.**. With next generation battery technologies, the aim is to increase metrics such as capacity, safety, and sustainability. This requires a search for novel electrode materials, electrolytes, and cell chemistries, including using alternative ions. Potential candidate ions to be used in batteries are Na and K which have low reduction potentials -2.71 V and -2.93 V respectively, and such chemistries are receiving increased attention by the research community.[11,12]

Table 1 Summary of Next Generation Battery Technologies

Technology	Advantages
Na-ion	Similar to Li-ion[13], low cost of Na[14], abundance of Na[14]
Li-S	High energy density[15], low cost of S[10], abundance of S[16]
Li-O_2	High energy density[15], abundance of O_2
Na-S	High energy density, low cost of materials, abundance of materials[14,17]
Mg	High energy density[18], abundance
Ca	Low cost, high abundance[19]
Al	High energy density[20], abundance

To address the issues of safety, cost, and extended capacity, Lithium-Sulfur and Sodium-Sulfur chemistries have considerable potential. Both Li-S and Na-S take advantage of the high capacity sulfur cathode, to take full advantage of this high capacity cathode the cell would need a high capacity anode. Despite the Na-metal anode having a slightly lower capacity of 1166 $mAhg^{-1}$ than its Li-metal counterpart, which has implications when the cell is balanced, the Na-S battery carries the advantage of the abundance of sodium. However there are issues of high Na-metal reactivity and poor room temperature performance of Na-S cells.[21] In this work, it is the Lithium-Sulfur chemistry that has been studied.

The Li-S reaction has a theoretical specific capacity of 1672 $mAhg^{-1}$ and an energy density of 2500 $Whkg^{-1}$ which has given the chemistry great interest. This high active material energy density has the potential to realise high energy densities on the cell level that surpass that of current Li-ion batteries.[22,23] There are also other factors that make the Li-S an ideal successor to Li-ion, including the abundance of materials, cost of materials, low-toxicity, and safety of the cell.[24]

In a Li-S cell, sulfur is used in its elemental form, S_8, this is an abundant material that is 10th in a ranking of elemental abundances,[25] it can be found worldwide making it accessible,[26] and often is the side product from established chemical processes, making it a very low cost material.[10] When you combine this with other elements to be used in the Li-S cell, such as carbon black, there is the potential to create a cell that has considerably lower cost materials than Li-ion cells. Sulfur-containing electrodes are considered to be less toxic,[10] an advantageous property considering the possible implementation of large scale applications. We are already seeing the potential environmental impacts of current battery use, from the way raw materials are mined, to what may happen to our battery materials in the case of combustion. Therefore, reducing the toxicity of our battery system can only be seen as advantageous.

3 Lithium-Sulfur

Having spoken in of the advantages of the Li-S chemistry, one must also consider the series of challenges which are preventing the implementation of this technology. These challenges stem from the complex chemistry that occurs in the Li-S cell. The overall cell reaction that is:

$$2Li^+ + 2e^- + S \rightarrow Li_2S \qquad \text{Equation 6}$$

The chemistry of the Li-S system differs from that of the currently used Li-ion batteries which are based on intercalation chemistry, where the Li^+ ions are inserted into layered materials. Instead, the cell's reaction mechanism can which can be broken down into a series of conversion reactions of sulfur[27] shown as follows:

$$S_8 + 2e^- + 2Li^+ \rightarrow Li_2S_8 \qquad \text{Equation 7}$$

$$Li_2S_8 + 2e^- + 2Li^+ \rightarrow Li_2S_{8-n} + Li_2S_n \qquad \text{Equation 8}$$

$$Li_2S_n + (2n-2)2e^- + (2n-2)Li^+ \rightarrow Li_2S_{8-n} + nLi_2S \qquad \text{Equation 9}$$

These reactions all contribute to the total capacity of the cell, and occur at different stages of the discharge process, Figure 6. The voltage profile in Figure 6 is typical of the dissolution-precipitation, which occurs when using a liquid electrolyte. The profile can be broken into 3 main regions and determined by corresponding processes, for simplicity we will discuss these processes with reference to cell discharge ($S_8 + 16e^- + 16Li^+ \rightarrow 8Li_2S$).

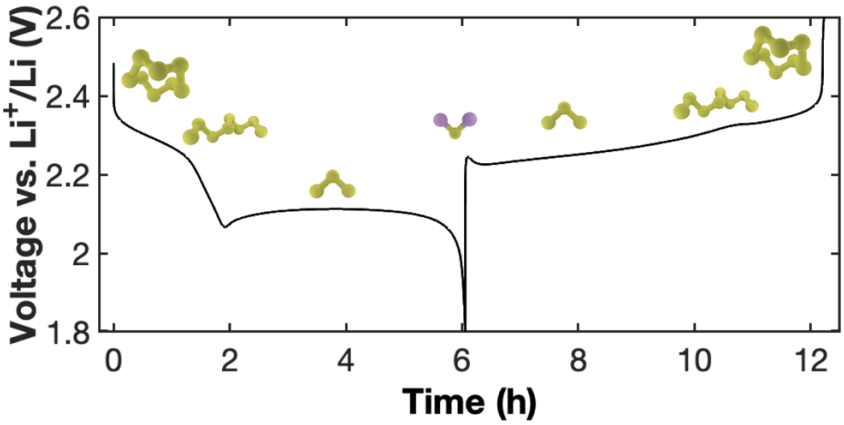

Figure 6 LiS voltage profile showing sulfur species present at different stages of discharge and charge.

At the start of discharge the conversion of elemental solid sulfur (S_8) to soluble high order polysulfides (Li_2S_8), equation 7, occurs and is a solid to liquid phase transition since elemental sulfur has a low solubility in commonly used electrolytes. Subsequently the conversion of the soluble long polysulfide chains to shorter polysulfide chains occurs, equation 8, and is a liquid to liquid transition. Finally, the conversion of short polysulfide chains (Li_2S_n) to insoluble lithium sulphide (Li_2S), equation 9, this is a liquid to solid phase transition. It is these phase transitions, and the use of the Nernst Equation that explain the characteristic shape of the voltage profile with liquid electrolytes.

Equation 7 represents the process at the plateau close to 2.4V in Figure 6, then equation 8 related to the slope moving from 2.4V-2.1V, and finally, equation 9 is represents the plateau at 2.1V. What is notable about the 2.1V plateau is the drop in the cell potential at the start of the 2.1 V plateau, which represents the energy needed to nucleate solid products on the electrode surface. The then deposited Li_2S, just like sulfur, is an electronic insulator that has the ability to block the carbon electrode surface and after a time prevent further deposition of discharge products, thereby significantly limiting the cell's capacity.[28]

3.1 Polysulfide Shuttle

All Li-S cells with the dissolution-precipitation reaction show the movement of Li_2S_n species, polysulfide shuttling. The shuttle occurssince the dissolved polysulfides are able to migrate to the lithium anode where they gain electrons from the lithium metal, they are reduced, and then migrate back to the cathode, illustrated in Figure 7. This means that polysulfide species can be reduced without accepting an electron from the cathode. In doing so the efficiency of the cell is limited, as the shuttle acts as an internal short circuit where polysulfide species gain an electron directly from the lithium. Other issues caused by the polysulfide migration are capacity fade due to polysulfide species being deposited on the lithium metal anode, active material loss, and also self-discharge of the cell rendering it incapable of long-term energy storage.

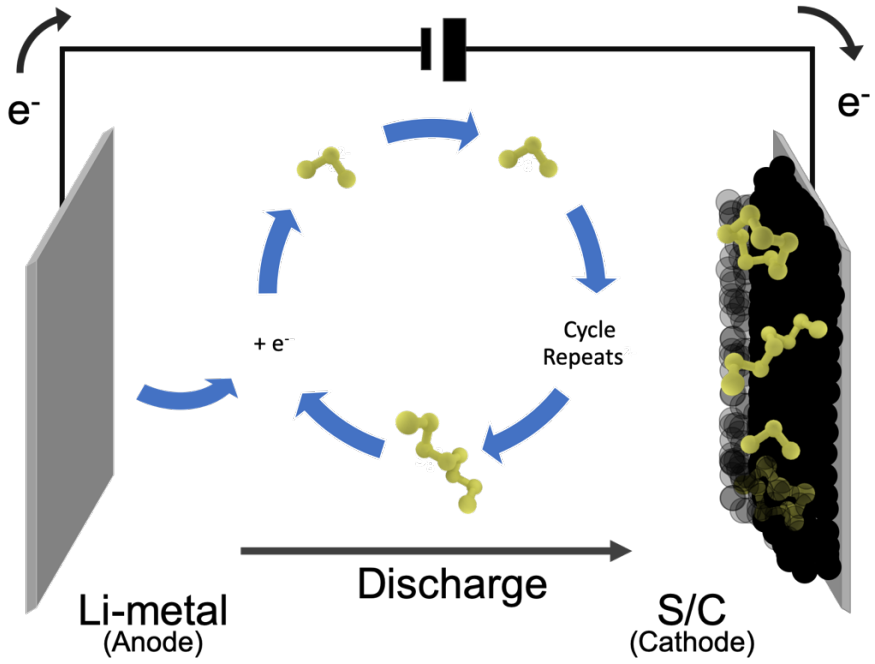

Figure 7 Schematic of polysulfide shuttle in a Li-S cell.

There are strategies that address the polysulfide dissolution and migration, such as sulfur confinement within hosts,[29–32] and the use of physical interlayers to block polysulfide movement.[33,34] Other methods mainly focus on the passivation of the Li-metal anode, the most common form of passivation is the use of lithium nitrate ($LiNO_3$) as an additive in the electrolyte. $LiNO_3$ breaks down and forms a passivation layer that allows the conduction of Li^+ ions through it, while at the same time protects the metal from shuttling species.[35,36] However, the solid-electrolyte interphase (SEI) formed with $LiNO_3$ breaks down continuously with unwanted side reactions during cycling and thus needs to be replenished. The constant replenishment of the SEI consumes $LiNO_3$ eventually leading to cell failure. For this reason $LiNO_3$ is referred to as a sacrificial salt, and in cells that rely on the use of this additive, there is an intrinsic link between its concentration in the electrolyte, the volume of electrolyte used, and the cell lifetime.[37]

3.2 Cathode

For the Li-S cell to operate effectively, the cathode must be a mixture of sulfur and a conductive matrix, often carbon, since sulfur by itself is an insulator.[38] The formation of a composite counters this challenge by creating a conductive matrix that surrounds the sulfur. The idea of a Li-S cathode was first conceived in a 1962 patent application[39], moving forward, work performed in 2009 by *Ji et al.*[40] proved it was possible create nanostructured cathodes that behave as polysulfide reservoirs, confining the soluble species within nanopores, enabling high efficiency and long lifetime Li-S cells.[40] This work on sulfur confinement has been further realised in work by She *et al.* where sulfur was encapsulated within TiO_2 shells, in a so-called 'yolk-shell' nanoarchitecture.[32] This method confined polysulfide species within the cathode, enabling a cycling for over 1000 cycles and maintain a high Coulombic efficiency, and is one of several confinement examples. [29–31]

The addition of carbon and a binder to the sulfur, leads to lower energy densities on the cell level. There have been recent efforts to create Li-S cells that are binder-free using self-standing carbon supports in an effort to reduce cell components and to raise the energy density.[22,41] When designing cathodes for a lithium sulfur cell, one must also consider the issue of volume expansion, the 80% volume increase from S to Li_2S must be accommodated in the cathode structure, and the cathode must have enough surface area and pore volume to accommodate the deposition of Li_2S during discharge, in an attempt to achieve the cell's full capacity.

3.3 Anode

To take advantage of the high capacity of sulfur, we need to couple it with a high capacity anode. The conventional graphite anode used in Li-ion batteries is not suitable since it has a theoretical specific capacity of 372 $mAhg^{-1}$. There are other potential anode candidates such as the use of a silicon anode with a high theoretical specific capacity of 4200 $mAhg^{-1}$, however, this system suffers from a large volume expansion of up to 400% which eventually leads to lower cycle lifetimes.[42]

A more suitable anode to be used in the Li-S system is simply lithium metal. The lithium metal anode has a high theoretical specific capacity of 3862 $mAhg^{-1}$ and the ability to produce a high-power cell. However, the Li-metal itself has challenges that can cause low performance of the Li-S system. The most notable issue posed by a lithium metal anode is that of dendrite growth. On the surface of the lithium metal there is a SEI, under this SEI lithium grows forming dendrites, eventually dendrites reach such a size the SEI cannot suppress them and they break through, reacting with the electrolyte and leads to low coulombic efficiencies. In the worst-case scenarios, these dendrites grow to such a size that they cause internal short circuits, rendering the battery inoperable or potential ignition of the cell.

3.4 Electrolyte

There is a wide range of electrolytes that have been applied to the Li-S cell, ranging from their chemistry and mechanisms, to the performance they yield.[43] The most notable of liquid electrolytes are the glymes (dimethoxyethane, tetraethylene glycol dimethyl ether), these glymes favour the dissolution of sulfur and cells with this type of electrolyte typically follow the dissolution-precipitation type reaction mechanism, discussed previously (Equations 7-9). Other types of electrolyte are catholytes (where the cell's active material is dissolved in the electrolyte), ionic liquids, solvated ionic liquids, and various types of solid electrolyte. All of which have their own advantages and flaws.

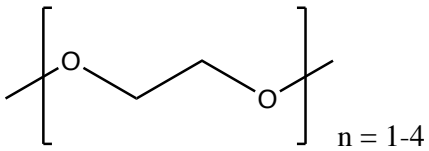

Figure 8 Structure of glymes

A favoured glyme based electrolyte is a binary mixture of the glyme 1,2-dimethoxyethane with 1,3-dioxolane, and the addition of salts. A commonly used salt for Li-S cells is Lithium bis(trifluoromethanesulfonyl)imide (LITFSI), a concentration of 1M is used to reach an ionic conductivity of 10^{-2} Scm^{-1}. The use of ethers and glymes leads to the previously mentioned dissolution-precipitation reaction mechanism as glymes favour the dissolution of soluble polysulfide species into the electrolyte. The dissolution is paramount to provide acceptable reaction kinetics at room temperature and to reach a high utilisation of the active material.

In clear contrast to the use of glymes is the use of a solid electrolyte and moving to an all-solid-state mechanism. This is most notably seen from the voltage profile of an all solid-state cell, where there are no plateaus, instead only a decaying voltage suggesting that no phase change occurs. There is very little information on the specifics of the mechanisms in an all-solid-state cell. A recent study by *Pang et al.*[44] showed that the solid state conversion of S_8 to Li_2S occurs via an Li_2S_4 intermediate, however this work was performed in a solvate ionic liquid electrolyte to induce a so-called 'quasi-solid-state' mechanism. As such the true discharge mechanism for all-solid-state Li-S cells is still relatively unknown, however, sulfide based solid electrolytes have been shown to enable specific capacities of 1600 $mAhg^{-1}$ at room temperature[45,46]. Challenges for solid electrolytes still remain such as dendrite formation through the solid structure, slow kinetics and high interface resistance. Solid electrolytes carry many advantages over traditional liquid type electrolytes, such having a wider electrochemical stability window, greater thermal stability, and reduced flammability.[47] However, most importantly, a consequence of the all-solid-state battery is that polysulfide species are confined to the cathode, if they are at all formed. In the solid state, any polysulfides that are formed would be unable to migrate from the cathode to the anode as they are physically blocked, thus preventing the parasitic shuttle mechanism.[48]

3.5 Catholyte

A Li-S system that is often based on a glyme type electrolyte, is the catholyte cell. A catholyte is an electrolyte with the active material dissolved in it, cathode + electrolyte = catholyte. Mixing Li_2S and S in a stoichiometric ratio in a solvent will form a polysulfide solution, the solution at this point turns a characteristic maroon colour. A catholyte can also be used in conjunction with a regular carbon-sulfur composite cathode, in this case the catholyte buffers the dissolution of sulfur.[49] A further approach commonly combines the catholyte with a sulfur-free cathode and has the ability to overcome issues such as cathode mechanical failure. The catholyte also enables cells to reach high areal capacities,[41,50] and can also create so-called 'synergetic systems, where the active material acts as a charge carrier replacing the need for LiTFSI in a cell.[51]

For catholyte based Li-S cells, a range of specific capacities have been reported, but the main advantage is high sulfur loading Agostini *et al.*[52] and Cavallo *et al.*[41] reported a sulfur loading of 3.2 $mgcm^{-2}$, Lim *et al.*[50] reported a sulfur loading of 6.5 $mgcm^{-2}$, and He *et al.*[53] reported loadings reaching 10 $mgcm^{-2}$. When compared to pioneering work by Pang *et al.* (4.6 $mgcm^{-2}$) and [54] Chung *et al*. (12 $mgcm^{-2}$, 46 $mgcm^{-2}$),[55] one sees a huge increase in loadings, while the authors claim to maintain a low electrolyte to sulfur ratio.[56] However these latter C/S cathodes require the use of materials such as cobalt and titanium disulphide. In stark contrast, the efforts by Cavallo *et al.,* and Lim *et al.* make use of carbon-based materials such as carbon nanofibers and reduced graphene oxide aerogels in combination with LiTFSI-free electrolytes, a potentially more sustainable and safer route for Li-S systems, not only in terms of raw materials needed to build these cells but also in terms of final cell cost. However, many of these catholyte cells still suffer from specific capacities not reaching their full potential, with poor rate capability and low active material utilisation.

3.6 Mechanistic Studies

There are have been many mechanistic studies performed to analyse the chemical processes in the Li-S cell, looking at the behaviour of sulfur and polysulfide species during charge and discharge. Techniques include X-ray tomography[57] and diffraction,[58–60] which gathers metrics such as the particle size distribution of sulfur in the cell's cathode, and also determines the crystal structures of sulfur during operation. Further techniques include Raman spectroscopy,[59,61–63] UV-vis spectroscopy,[64–66] X-ray absorption spectroscopy,[67] and Electron Paramagnetic Resonance spectroscopy[68] which are are able to track the speciation of sulfur in a cell's electrolyte, or in the electrode.

Pioneering work by *Tan et al*[57]. has shown the evolution of sulfur particles during cell discharge and charge. By using synchrotron tomography, the sizes of all sulfur particles within the entire cathode volume were tracked and compared with depths of discharge. This provides a key insight into how the distribution of sulfur particles changes with cycling, what the potential effect or porosity is, and evaluates this information with regards to electrochemical cycling.

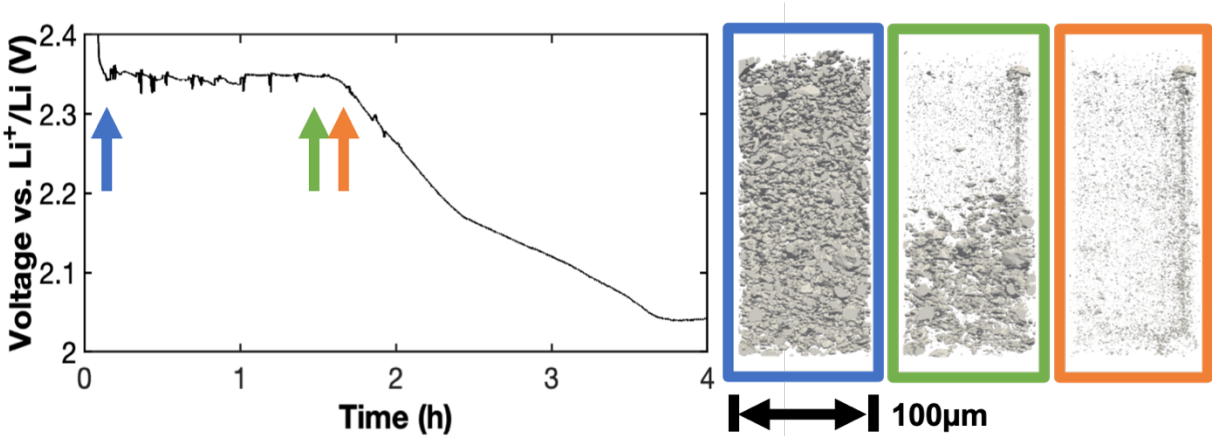

Figure 9 X-ray Reconstruction of sulfur inside a C/S at different stages of discharge for a cell discharged at a rate of C/10. Data gathered from the TOMCAT beamline at PSI Switzerland in a joint project with the Technical University of Denmark, reconstructions courtesy of Salvatore De Angelis.

One example of how X-ray tomography can be used is shown in Figure 9, where we see tomographic reconstructions of sulfur particles within a composite sulfur carbon cathode. This data comes from experiments performed on the Swiss Light Source's TOMCAT beamline at the Paul Scherrer Institute in a joint project with the Technical University of Denmark. From the reconstructions a clear dissolution path of sulfur is seen, as sulfur dissolves from the top of the cathode. It dissolves at a seemingly non-linear rate, suggesting the issues of cathode 'wetting' and electrolyte super-saturation being important effects on the cell's kinetics. However, this technique has its limitations in terms of providing information on the mechanism of the cell, due to the resolution being in the range of micrometres. As such, only relatively large sulfur particles can be followed during cycling and dissolution. Once the sulfur has dissolved and formed soluble polysulfide species we can cannot observe their subsequent reduction in solution, nor the deposition of Li_2S which will have smaller particle sizes.

Further methodologies used to characterise solid products in Li-S cells, include the use of X-ray diffraction. Here the crystal structures of S (both α and β) and Li_2S can be determined, showing at which depths of discharge and charge such species are consumed/formed. However, this technique is limited by the fact it is unable to directly demonstrate the effect of cathode structure on the dissolution and formation of these products. Additionally, lab source x-ray techniques typically need long measurement times, on the order of hours, making these techniques unsuitable for *operando* measurements by not providing high temporal resolutions. To perform *operando* x-ray experiments, synchrotrons provide fast measurement times, allowing the smallest changes in Li-S chemistry to be captured.[69]

To characterise soluble species in the liquid phase optical techniques are the most popular choice due to being lab based, having an ease of application, and having short measurement times. ,[59,61–66] However, other techniques also used to analyse the liquid phase include XAS[67] and EPR.[68] The way the liquid-liquid reactions are presented in equation 8 is a simplification, with not all polysulfide conversions being faradic processes. There are also chemical disproportionation reactions that play an intrinsic part of the lithium sulfur mechanism, such as the one shown in equation 10. These varying polysulfide species have been tracked by the previously mentioned techniques, trying to observe changes in their concentration and effectively determine the pathway sulfur species take during discharge and charge. Such an understanding is enabled by rapid measurements that provide decent time resolutions and give detailed insights to the smallest changes in the discharge mechanism.

$$S_6^{2-} \leftrightarrow S_3^{*-} \qquad \text{Equation 10}$$

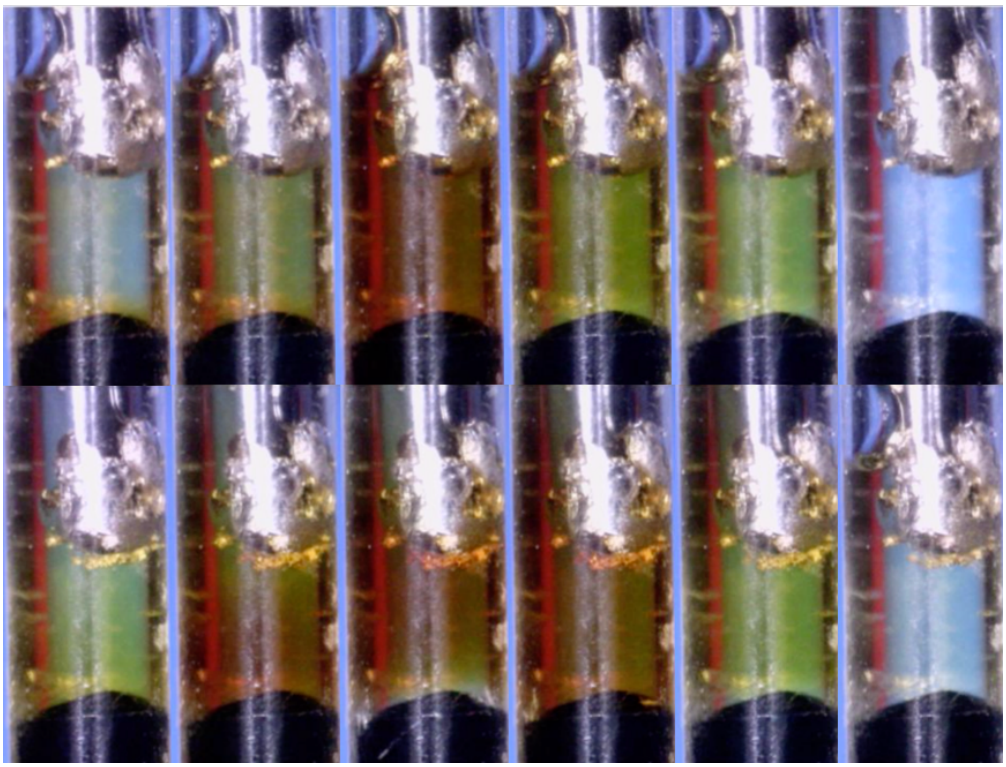

Figure 10 Polysulfide changes with respect to DoD (top row) and DoC (bottom row). Data gathered in a combined project with the Technical University of Denmark, images courtesy of Didier Blanchard.

However, such techniques are limited by their spatial resolution, with EPR and UV-vis gathering information on the bulk electrolyte in custom cells, and Raman spectroscopy only being able to provide information from a confined area, once again in custom cells. This is useful only if reactions at the anode or cathode are to be probed, but a limitation in terms of tracking interactions across the entire electrolyte volume. It can clearly be seen from Figure 10 that polysulfide species show a unique behaviour in the way that they diffuse through the cell during discharge and charge, this movement has implications on the mechanism as not only do the species move from the cathode to the anode, but they are still redeposited on the cathode. By only measuring bulk solutions, or by measuring at one point in the cell, the true lithium sulfur mechanism is lost. Other limitations stem from the inability of each technique to only identify a set number of polysulfides. An example is how Raman spectroscopy detects different polysulfide species depending on the wavelength of incident laser used, we know this from the response of polysulfides to UV-vis spectroscopy.[64–66] Despite its previously mentioned limitations, Raman spectroscopy is a particularly powerful tool for identifying various chemical bonds present in a sample, and it has even been shown that it is possible to discriminate against different polysulfide species,[59,61,62] making this technique particularly well suited to probe the Li-S system in order to precisely identify the polysulfide species and deepen the understanding of polysulfide interactions.

Understanding the polysulfide speciation and Li_2S formation provides further insights to the mechanisms of the Li-S cell. This information can be used to create physical models for the Li-S system,[70] to determine cell kinetics, determine how to tune the electrolyte to favour given polysulfide species, and to tune the electrode properties to improve kinetics. However, the multitude of Li-S systems under investigation differ vastly in the processes that occur, and how sulfur interacts with the various components of the cell, and no single technique can identify all the processes occurring at once.[69,70] Huge scope has been left for further insights to the lithium-sulfur cell, not only to investigate the speciation of sulfur, but also to learn the effect of electrolyte composition on sulfur speciation.

The catholyte concept previously introduced is widely used and offers a different mechanism from a ‘standard’ Li-S configuration that uses carbon/sulfur composite cathodes. Instead of there being an initial stage of sulfur dissolution, in catholyte, the cell’s pristine state is one where all sulfur is initially dissolved. This has implications of a diverging mechanism due to the increased polysulfide presence. Implications that ask the questions: How do the polysulfides interact with the electrolyte? How do polysulfides migrate through the cell? How does the use of polysulfides as the Li-salt affect their interactions in the cell? All questions that need answers to develop a further understanding of the behaviour of polysulfide species. This work aims to understand the interaction between polysulfides and salts in catholyte cells, and why their interactions may affect the mechanisms of catholyte type Li-S cells.

4 Theory and Experimental

4.1 Electrochemical Techniques

4.1.1 Cyclic Voltammetry

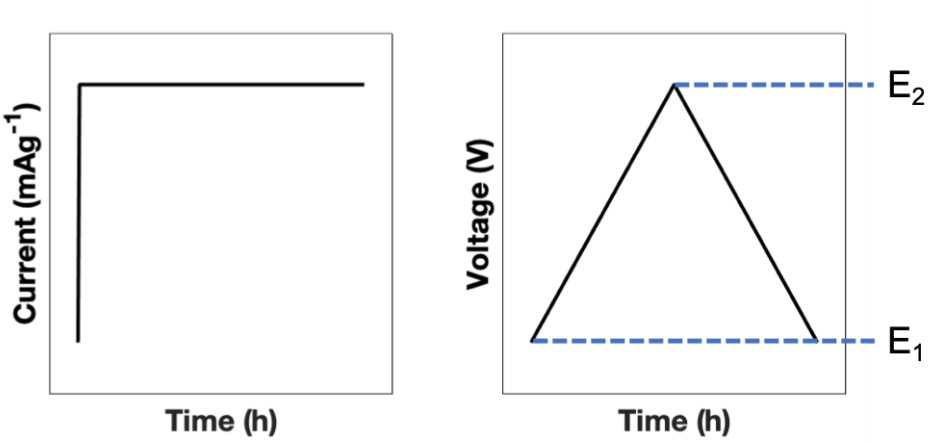

Figure 11 Schematics showing current and potential control in Galvanostatic Discharge/Charge and potentiostatic Cyclic Voltammetry.

Cyclic voltammetry is used for electrochemical analysis, is a potentiostatic measurement where the potential is controlled, and the current response is measured. The cell voltage is swept between two potential limits (E_1 and E_2) as shown in Figure 11, and the current response is recorded. Typically, cyclic voltammetry reveals redox processes that occur within a system, and for batteries cyclic voltammetry will reveal the potential at which chemical conversions in the electrolyte occur. Data from cyclic voltammetry has current, or current density, plotted as a function of potential, hence giving a cyclic plot showing successive cycles.

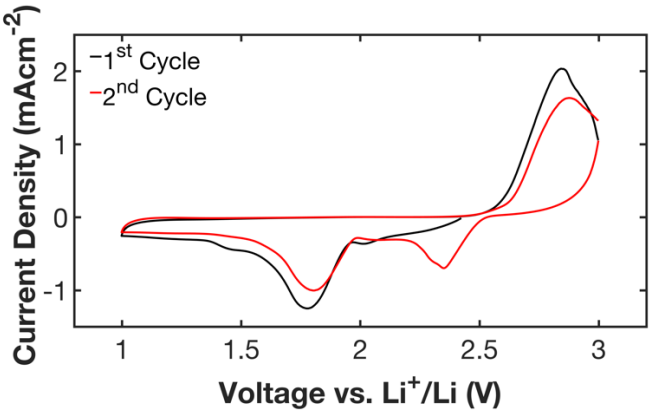

Figure 12 Example Cyclic Voltammogram for a Catholyte system, showing the reduction peaks which represent the conversion of S_8 to Li_2S_n (~2.4V) and subsequent conversion to short Li_2S_n chains (~1.8V).

4.1.2 Galvanostatic Discharge/Charge

To evaluate full and half cells, galvanostatic constant current charge-discharge (CC) measurements are used. Here a current is applied at a given rate (mAg^{-1}), and the voltage response is measured, with voltage limits being applied. These measurements provide information on capacity, rate capability, and Coulombic efficiency. Typically for such measurements data is reported showing voltage as a function of time or capacity, as shown in Figure 13.

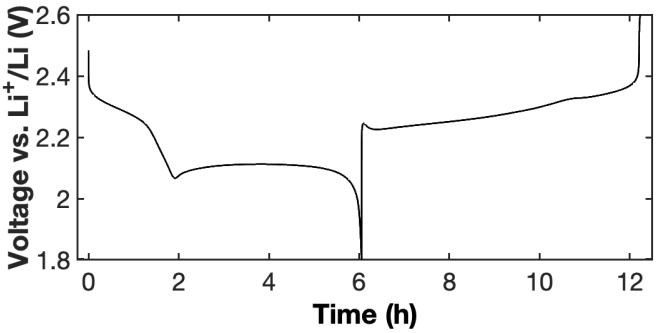

Figure 13 Example Li-S Galvanostatic Voltage Profile.

Furthermore, CC measurements can be used to test the stability of electrolytes against lithium metal, which is used as the anode in Li-S cells. By applying a constant current density to a symmetric Li-Li cell, we drive lithium stripping and lithium deposition processes, much as we would have in our working cell. By applying a current and inducing this process, the voltage response can be measured, in this case, the overvoltage. This overvoltage represents the driving force of the oxidation/reduction process (stripping/deposition respectively), thus a higher overvoltage means a higher resistance and poorer stability of the lithium in a given electrolyte, this effect is illustrated in Figure 14.

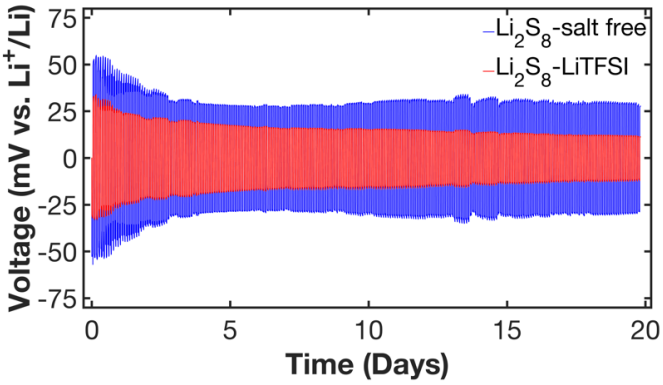

Figure 14 Example of a stripping/deposition measurement used to evaluate two different catholyte solutions.

4.2 Raman Spectroscopy

Raman spectroscopy is a useful tool for identifying vibrational modes in materials. First discovered by C.V. Raman in 1928[71], it is the inelastic scattering of light by matter, showing that there has been a change in energy between incoming and outgoing photons, equivalent to the energy of a vibrational mode.

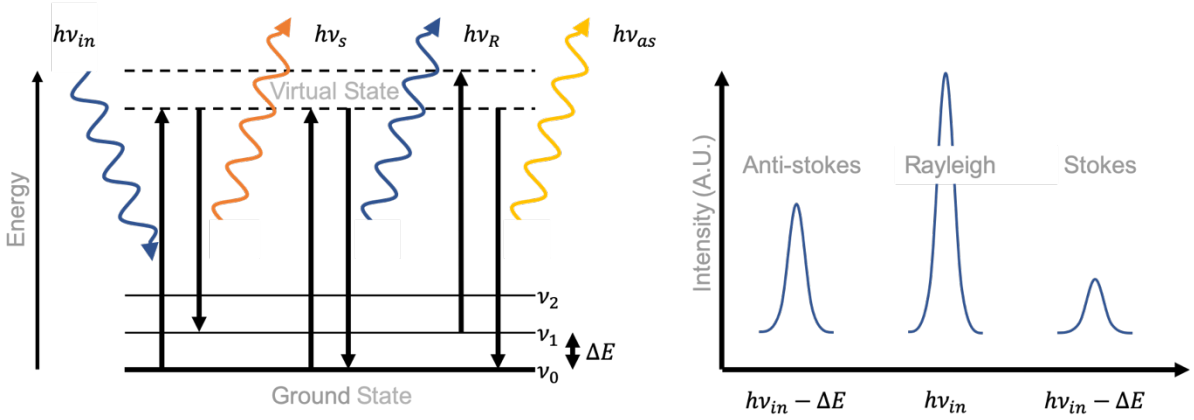

Figure 15 Jablonski Diagram of the Raman Scattering process and related appearance of a spectrum.

In Raman spectroscopy, monochromatic light, frequency υ_L, impinges on a sample. If the energy of this light is lower than the energy needed to change electronic states, then the molecule will be excited to a 'virtual state'. When the molecule decays from the virtual state a photon will be emitted with an energy $h\upsilon_{in} \pm \Delta E$ with ΔE being the difference in energy between ground and excited vibrational states. Through this process we can have three different cases of scattering as seen in Figure 15. The first is Raleigh scattering this is where the light is elastically scattered, i.e. the emitted photon has the same energy as the incident photon. Thus, there is no change in energy and the frequency of Rayleigh scattering is the same as the incident frequency. The second type of scattering is known as Stokes scattering. Stokes scattering is inelastic scattering where the molecule starts in a ground vibrational state and ends in excited virtual state. The energy of the emitted photon is shown by equation 11, this corresponds to light shifted to lower frequency compared to the frequency of the incident light.

$$h\upsilon_s = h\upsilon_{in} - \Delta E \qquad \text{Equation 11}$$

The third type of scattering is anti-Stokes scattering, Anti-Stokes scattering is also inelastic scattering, but here the molecule starts in an excited vibrational state and ends in the ground state. The energy of the emitted photon is shown by equation 12, this corresponds to light shifted to higher frequency compared to the frequency of the incident light.

$$h\upsilon_{as} = h\upsilon_{in} + \Delta E \qquad \text{Equation 12}$$

In both Stokes and Anti-Stokes scattering, the change in energy is due to the difference in energy between the vibrational energy states ν_0 and ν_1, this difference in energy can be considered as the energy from a vibrating chemical bond. In a bond the frequency of the vibration is dependent on the mass of the atoms in a bond as defined by the reduced mass:

$$\mu = \frac{m_1 m_2}{m_1 + m_2}$$ Equation 13

Once we know the reduced mass and the bond force constant (bond strength) of a given molecule we are able to calculate the vibrational frequency:

$$\nu = \frac{1}{2\pi}\sqrt{\frac{k}{\mu}}$$ Equation 14

Vibrations can be divided in symmetric and anti-symmetric, depending if the motions of two (or more) atoms involved in the vibration are symmetric or not. Moreover, vibrations are usually divided in the following way: stretching (vibration in the same direction of an atomic bond), bending (oscillation that implies a change of angle between two atomic bonds), rocking (oscillation that implies a change of angle between a group of atoms), wagging (change in angle of the plane of a group of atoms), twisting (change in angle of the planes of two groups of atoms). There is a selection rule for which vibrational mode are Raman active. For a mode to be Raman active there needs to be a change in polarizability as the molecule vibrates, described by:

$$\mu_{ind} = \alpha E$$ Equation 15

Here μ_{ind} is the induced dipole, α is the polarizability of the molecule, and E is the electric field; we need this polarizability to induce a time dependant dipole moment which is crucial to the Raman effect. For a more complete description of Raman spectroscopy please see the text by *Larkin*.[72]

4.2.1 Confocal Raman Spectroscopy

In combination with a commercially available *in situ* cell from EL-CELL,[73] Raman measurements were made using a confocal Raman spectrometer. In confocal measurements scattered photons are only recovered from a focal plane, meaning that specific points as a function of depth in the cell can be probed (e.g. electrolyte or the surface of materials in the cell). This technique is particularly useful for identifying concentration changes of polysulfide species in localised regions of the electrochemical cell. In data presented in Paper III, the polysulfide species are identified near the anode, giving us further insights into the mechanisms of this lithium-sulfur catholyte cell.

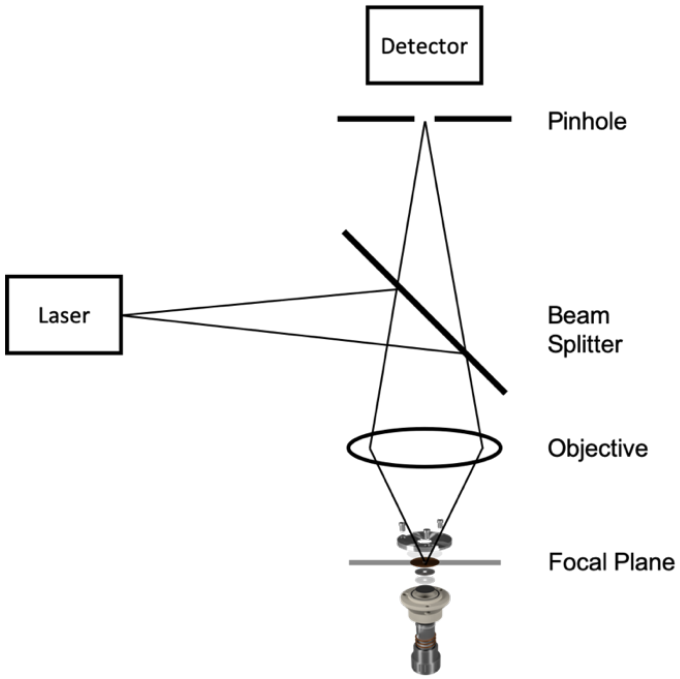

Figure 16 Schematic of confocal Raman experimental setup.

Using a specifically designed *in situ* cell shown in Figure 17, it is possible to collect Raman spectra, exhibiting the chemical environment in the lithium-sulfur cell during cycling, a so called *operando* methodology. Raman spectroscopy is particularly well suited to perform *operando* measurements on the Li-S system, due to its non-destructive nature allowing data acquisition over multiple cycles, and the speed of spectrum acquisition is comparable with relevant discharge/charge rates.

The *in situ* cell allows cyclic voltammetry or constant current charge/discharge experiments to be performed in conjunction with Raman. Figure 17 shows the design and component arrangement in the *in situ* cell used in Paper III.

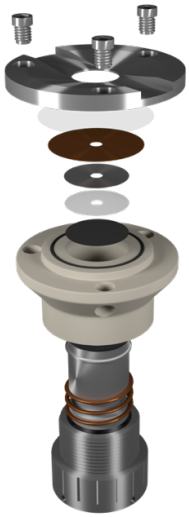

Figure 17 Design and electrode format in the *in situ* cell. From bottom up: carbon working electrode, glass fibre separator, lithium metal, copper current collector, glass window.

Operando measurements are often accompanied by trade-offs that are an effect of performing measurements on a dynamic system. Often, *in situ* cells have higher internal resistances which affect the voltages seen for a given process, the cell has to be designed in such a way that the materials being probed are in close proximity to the optical window, meaning that only one component of the cell can be analysed in a given measurement. In terms of measurements, spectra must be recorded rapidly in order to provide an accurate representation of the cell chemistry at a given point during cell discharge/charge, in addition to using the correct laser wavelength and intensity, which must be carefully selected to supress fluorescent background effects and not heat cell components. These aspects are often in competition with trying to obtain an acceptable signal to noise ratio and will vary from system to system.

5 Results and Discussion

The following section highlights the results from the appended papers (I-III), all papers focus on the interactions between sulfur and the electrolytes used. These interactions focus on how the electrolyte can be tuned to supress polysulfide dissolution and enable cells that have long cycle lifetimes, as seen in Paper I. Then also target how polysulfides can be used in the electrolyte to prevent the breakdown of the cathode structure, and once more enable cells with long cycle lifetimes and high energy densities (Paper II). Finally, we investigate how the electrolyte composition can affect the speciation and distribution of polysulfides within a cell and enable cells to reach a higher capacity (Paper III).

5.1 Methods to Prevent Polysulfide Shuttle

Section 3.1 highlights how the polysulfide shuttle can be supressed through the addition of $LiNO_3$ as additive, which forms a stable SEI, preventing polysulfide species from reaching the Li-metal surface and being reduced. However, the $LiNO_3$ additive is continuously consumed, it will eventually be depleted at this point the cell will begin to fail, and this challenge is addressed in Paper I, as illustrated in Figure 18. After 150 cycles, both the Coulombic efficiency and the specific discharge capacity for the electrolyte using $LiNO_3$ (orange) began to drop in value.

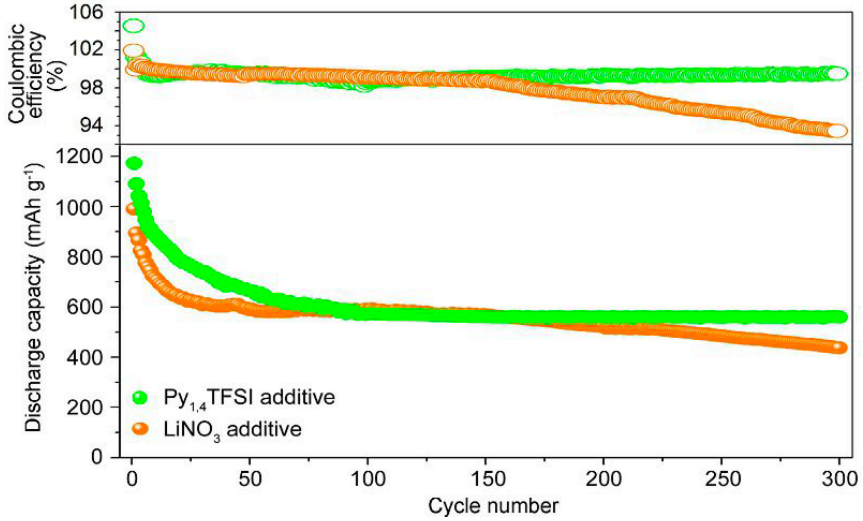

Figure 18 Prolonged cycling and coulombic efficiency comparison. Cycling rate C/30=56 mAg^{-1}; voltage cut-off: 1.4–2.8 V for the $Py_{14}TFSI$ cell and 1.8–2.8 V for the $LiNO_3$ cell. Figure 5 from Paper II.

The drop in Coulombic efficiency indicates that polysulfide species are shuttling. In addition, the cells discharge capacity began to drop after 150 cycles, suggesting a loss of active material directly linked to side reactions on the anode. In contrast, when using $Py_{14}TFSI$ as additive in the electrolyte, the cell maintains a high Coulombic efficiency, above 99%, and high discharge capacity up to 300 cycles, suggesting that a stable SEI was formed, and that this SEI has a longer lifetime than one that is formed by $LiNO_3$. This new SEI is polymeric in its nature and is the product of $TFSI^-$ decomposition. An additional difference between the cells with the two electrolytes can be observed. The cell with the $LiNO_3$ additive electrolyte shows a rapid capacity fade over the first 20 cycles suggesting rapid dissolution of the sulfur cathode, whereas the $Py_{14}TFSI$ additive shows a slower decay over 80 cycles, to reach a stable capacity of 600 $mAhg^{-1}$. The viscosity of the electrolyte is thought to slow down the dissolution of lithium polysulfide species and be the explanation of the observed behaviour.

5.2 Utilising Polysulfides for Long Life and High Energy Density Cells

Section 5.1 highlights the importance of protecting the Li-metal surface, with an SEI, and how choosing the correct electrolyte can impact the composition of this SEI and the subsequent lifetime of a cell. However, once a method has been chosen to passivate the Li surface, one can then utilise polysulfide species to improve cathode performance.

Paper II shows that using C/S composite cathode with a catholyte, in place of an electrolyte, there are two effects. The first is an increase in effective energy density. Since the catholyte used in this cell acted as a charge carrier, LiTFSI is replaced by polysulfide species in the electrolyte, leading to an increase in the amount of active material and a decrease in the electrolyte volume.

A second effect is that the sulfur present in the catholyte can buffer the dissolution of sulfur in the cathode, enabling cells of long cycle lifetime. Figure 19a shows that the cell under investigation retains 80% cell capacity after 500 cycles, while maintaining a Coulombic efficiency greater than 99%. The catholyte cell also contains $LiNO_3$ which prevents the shuttling of species present in the catholyte, however a high concentration of $LiNO_3$ has to be used due to the low electrolyte volume

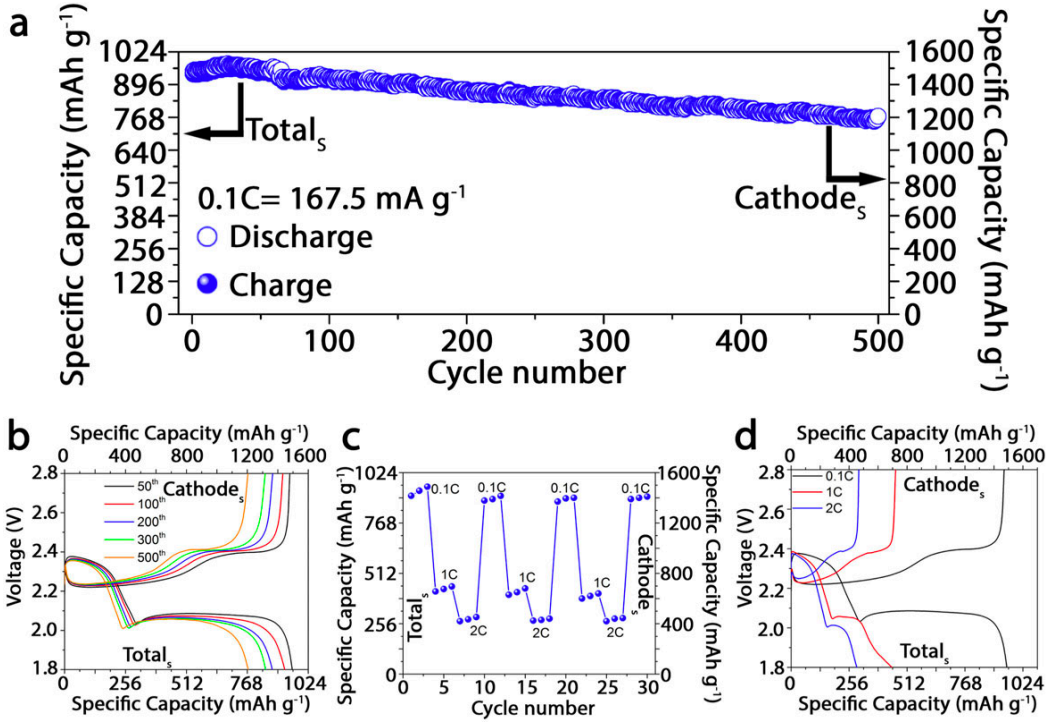

Figure 19 a) Prolonged cycling performance of the CMK3/S electrode in Li–S cells using DOL/DME–0.4M LiNO3–0.5M Li_2S_8 electrolyte at a current rate of 0.1 C=167.5 mAg^{-1} and b) corresponding voltage profiles at different cycles c) Rate capability step test from lowest current rate 0.1 C, to highest 2 C and d) corresponding voltage profiles.

However, Figure 19c highlights the limitations of this cell design, a poor rate performance. The cell is able to recover 95% of its capacity after the rate is increased to 2C and then returned to 0.1C, however when increasing the discharge rate to 2C there is a 74.4% reduction in capacity showing that further improvements are needed to ensure fast kinetics.

5.3 *Operando* Investigations of Polysulfide Speciation and Distribution

Section 5.2 highlighted that one of the advantages of a catholyte cell is that the traditional salt, LiTFSI, can be removed from the cell and the polysulfides themselves can act as the lithium salt and carry charge as well as contribute to the capacity. To investigate the changes in electrochemical mechanism, Paper III employed the use of two catholytes, one containing LiTFSI salt and one that was salt-free.

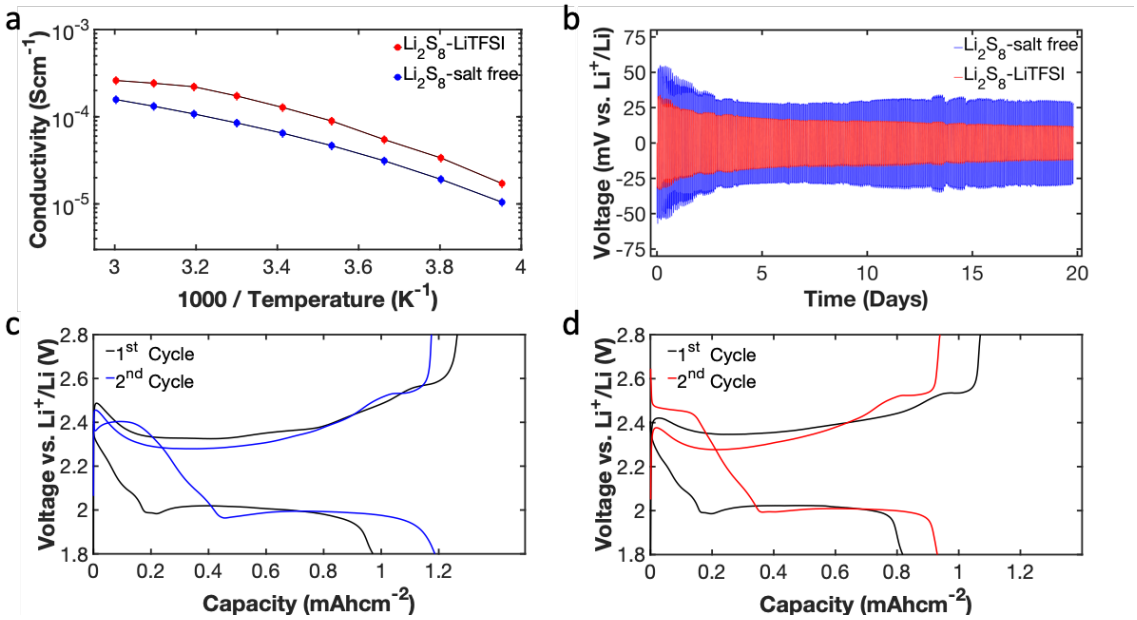

Figure 20 a) Arrhenius plot trends and b) Li plating/stripping measurements. Galvanostatic profiles at the 1st and 2nd cycles of c) Li_2S_8 salt-free and d) Li_2S_8 LiTFSI Li-S cells (current rate 0.3mA/cm^2 with Voltage limits 1.8V-2.8V).

Figure 20b shows the Li plating/stripping in a symmetric cell and the stabilisation of the two cells' respective overpotentials. Both systems show a rather stable overvoltage, without significant increase over 19 days, highlighting a good compatibility with the Li-metal anode thanks to the use of 0.4 M $LiNO_3$ to form a stable interface.[35] A noticeably lower overvoltage for the catholyte containing 0.5 M of LiTFSI was observed, while the salt-free catholyte shows a slight increase in overvoltage, related to the difference in ionic conductivity between the two electrolytes, Figure 20a.

Both cells show a 1st discharge voltage profile with a single plateau at ~2V, as there is the reduction of Li_2S_n polysulfides to Li_2S as seen in Figure 20c and Figure 20d. The cell using the salt-free catholyte solution shows a higher 1st discharge capacity compared to the cell using the LiTFSI catholyte, with both showing a 20% increase in capacity upon the 2nd cycle. We see from galvanostatic cycling that the salt-free catholyte outperforms the LiTFSI containing catholyte.

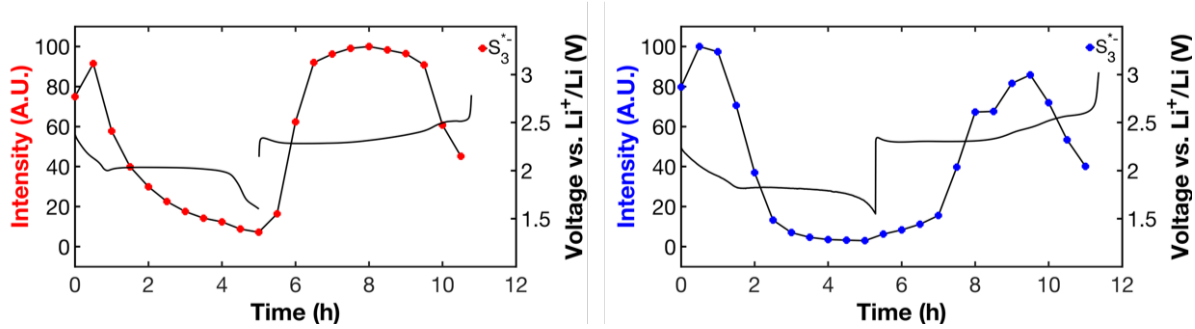

Figure 21 Peak intensity of 531cm^{-1} (S_3^{*-}) Raman shift plotted against galvanostatic voltage profile for the LiTFSI containing (red) and for the salt-free containing catholyte (blue).

Figure 21 shows the use of Raman spectroscopy to track the concentration change of the S_3^{*-} polysulfide. During the first discharge step, between 2.4 and 2.1V, there is a high increase in the S_3^{*-} radical intensity, normally the region where the conversion of Li_2S_8 and Li_2S_6 to shorter chain polysulfides occurs. The presence of S_3^{*-} is a signature that S_6^{2-} species are formed. At the start of the voltage plateau at 2.1V the intensity of the S_3^{*-} peak rapidly drops in the salt-free catholyte, Figure 21(blue). This result is consistent with a mechanism where there is a rapid migration of polysulfide species to the cathode as the end product Li_2S is formed and precipitated on the carbon support. In the case of the TFSI catholyte, the decrease in intensity of the S_3^{*-} band is much slower and continues during the whole discharge, Figure 21(red), in agreement with a more sluggish migration of polysulfide species through the electrolyte towards the cathode.

During charge the cell with the salt-free catholyte shows a very low concentration of S_3^{*-} close to the anode until the cell has reached 40% of full charge, Figure 21(blue). This behaviour is thought to be due to the formation of short chain polysulphides, up to Li_2S_4, and longer species are not formed until greater states of charge. The observation of the S_3^{*-} Raman band coincides with a higher plateau in the voltage profile which could indicate the formation S_6^{2-} which can disproportionate to S_3^{*-}. The Raman spectrum of the TFSI containing catholyte shows the S_3^{*-} Raman band intensity increase rapidly at the start of charge, Figure 21(red), pointing to a mechanism where long chain polysulfides are formed immediately.

6 Conclusions and Outlooks

The work in this thesis is centred around methods to manipulate and understand the behaviour of polysulfides at both the anode and cathode. Paper I demonstrates how at the anode polysulfide interaction was supressed by forming an SEI using a novel electrolyte, this SEI has a much longer lifespan than what would be seen with traditionally used electrolyte additives, and as such the cell demonstrates an enhanced cycling life. In addition, due to the concentration of LiTFSI, this novel electrolyte has a high viscosity where the solvents used are close to their solubility limits. Thus, the rate of dissolution of the sulfur cathode is reduced, leading to a slower capacity decay. It is then seen that by applying polysulfides as the Li-salt and using a reduced electrolyte volume that this capacity decay can be completely supressed. Paper II exhibits the buffering characteristics of polysulfide species in the catholyte, which in turn prevent dissolution of the sulfur solution and prevent capacity decay. After realising the use of polysulfides as Li-salts, *operando* Raman spectroscopy used in Paper III demonstrated a difference in cell mechanism when the polysulfides behaved as charge carriers. In this case, the movement of polysulfide species to the Li-metal anode is supressed and leads to more efficient polysulfide conversion process, in turn leading to an increase in cell capacity.

However, in these measurements, only polysulfides reaching the anode were observed and there is still the need to determine how polysulfides speciate through the whole cell and understand how solid products nucleate within the microstructures of cathodes. This speciation and distribution of polysulfide and solid species needs to be compared with metrics such as rate performance, eventually enabling us to design more efficient cathode structures and pave the way for high rate capable and high energy density cells.

7 Acknowledgements

First, I would like to thank the Swedish Energy Agency who have funded my work, and thanks to members of the STARC project who I have had many discussions with over these past years.

I would also like to thank my supervisor Aleksandar Matic, who first agreed to host me for my Master's Thesis back in 2016 while I was a student at the University of Southampton, and then went one step further to take me on as a Doctoral student. Since then you have provided me with many opportunities to explore the research field we are in and to a grow as a scientist. I will always be grateful for this.

To the many members of the Kondenserande Materiens Fysik research group here at Chalmers (affectionately known as KMF) who I have known over the years, you have all helped me in some small part. Whether that be you helping me get settled with my new life here in Sweden, helping me learn how to use equipment, or helping with discussions, you have all taken a role in my personal development.

I would also like to mention collaborators from The Technical University of Denmark, who I have worked with closely over the past year, you have been an endless source of knowledge and experience. I look forward to our continued collaboration in the coming years.

Finally, I would like to thank my friends, family, and my partner. All of who have given me support over these past 2 years, and I can only hope that I make you proud. However, I would like to take this moment to clarify that with my current skill set, I cannot increase the battery percentage of your phone.

8 References

1 K. Mizushima, P. C. Jones, P. J. Wiseman and J. B. Goodenough, *Solid State Ionics*, 1980, **3**–**4**, 171–174.

2 S. Chu and A. Majumdar, *Nature*, 2012, **488**, 294–303.

3 International Energy Agency, CO2 Emissions Statistics, https://www.iea.org/statistics/co2emissions/, (accessed 13 September 2019).

4 R. Logtenberg, J. Pawley and B. Saxifrage, *Comparing Fuel and Maintenance Costs of Electric and Gas Powered Vehicles in Canada*, 2018.

5 Siemens, Airbus and Rolls-Royce, Airbus, Rolls-Royce, and Siemens team up for electric future, https://press.siemens.com/global/en/pressrelease/airbus-rolls-royce-and-siemens-team-electric-future, (accessed 9 October 2019).

6 A. W. Schäfer, S. R. H. Barrett, K. Doyme, L. M. Dray, A. R. Gnadt, R. Self, A. O'Sullivan, A. P. Synodinos and A. J. Torija, *Nat. Energy*, 2019, **4**, 160–166.

7 D. Linden and T. B. Reddy, *Handbook of batteries*, McGraw-Hill, Third Edit., 1995, vol. 33.

8 D. Pletcher, *A First Course in Electrode Processes*, The Royal Society of Chemistry, Southampton, 2nd Editio., 2009.

9 A. J. Bard and L. R. Faulkner, *Electrochemical Methods*, John Wiley & Sons, Inc., 2001.

10 X. Ji and L. F. Nazar, *J. Mater. Chem.*, 2010, **20**, 9821–9826.

11 E. Irisarri, A. Ponrouch and M. R. Palacin, *J. Electrochem. Soc.*, 2015, **162**, A2476–A2482.

12 W. Luo, J. Wan, B. Ozdemir, W. Bao, Y. Chen, J. Dai, H. Lin, Y. Xu, F. Gu, V. Barone and L. Hu, *Nano Lett.*, 2015, **15**, 7671–7677.

13 A. Bauer, J. Song, S. Vail, W. Pan, J. Barker and Y. Lu, *Adv. Energy Mater.*, 2018, **8**, 1–13.

14 M. D. Slater, D. Kim, E. Lee and C. S. Johnson, *Adv. Funct. Mater.*, 2013, **23**, 947–958.

15 P. G. Bruce, S. A. Freunberger, L. J. Hardwick and J. M. Tarascon, *Nat. Mater.*, 2012, **11**, 19–29.

16 A. Manthiram, Y. Fu and Y. S. Su, *Acc. Chem. Res.*, 2013, **46**, 1125–1134.

17 Z. Wen, Y. Hu, X. Wu, J. Han and Z. Gu, *Adv. Funct. Mater.*, 2013, **23**, 1005–1018.

18 I. Shterenberg, M. Salama, Y. Gofer, E. Levi and D. Aurbach, *MRS Bull.*, 2014, **39**, 453–460.

19 D. Larcher and J. M. Tarascon, *Nat. Chem.*, 2015, **7**, 19–29.

20 Q. Li and N. J. Bjerrum, *J. Power Sources*, 2002, **110**, 1–10.

21 X. Xu, D. Zhou, X. Qin, K. Lin, F. Kang, B. Li, D. Shanmukaraj, T. Rojo, M. Armand and G. Wang, *Nat. Commun.*, 2018, **9**, 1–12.

22 M. Agostini, J. Y. Hwang, H. M. Kim, P. Bruni, S. Brutti, F. Croce, A. Matic and Y. K. Sun, *Adv. Energy Mater.*, 2018, **8**, 1801560.

23 M. Agostini, D. H. Lim, M. Sadd, J. Y. Hwang, S. Brutti, J. W. Heo, J. H. Ahn, Y. K. Sun and

A. Matic, *ChemSusChem*, 2018, **11**, 2981–2986.

24 M. Agostini, M. Sadd, S. Xiong, C. Cavallo, J. Heo, J. H. Ahn and A. Matic, *ChemSusChem*, 2019, **12**, 1–10.

25 Thomas Jefferson National Accelorator Facility, The Element Sulfur, https://education.jlab.org/faq/index.html, (accessed 14 September 2019).

26 U.S. Geological Survey, Sulfur, https://prd-wret.s3-us-west-2.amazonaws.com/assets/palladium/production/atoms/files/mcs-2019-sulfu.pdf, (accessed 14 September 2019).

27 S. S. Zhang, *J. Power Sources*, 2013, **231**, 153–162.

28 S. Xiong, K. Xie, Y. Diao and X. Hong, *J. Power Sources*, 2014, **246**, 840–845.

29 J. He, L. Luo, Y. Chen and A. Manthiram, *Adv. Mater.*, 2017, **29**, 1–5.

30 B. Zhang, X. Qin, G. R. Li and X. P. Gao, *Energy Environ. Sci.*, 2010, **3**, 1531–1537.

31 H. Wang, Y. Yang, Y. Liang, J. T. Robinson, Y. Li, A. Jackson, Y. Cui and H. Dai, *Nano Lett.*, 2011, **11**, 2644–2647.

32 Z. W. Seh, W. Li, J. J. Cha, G. Zheng, Y. Yang, M. T. McDowell, P. C. Hsu and Y. Cui, *Nat. Commun.*, , DOI:10.1038/ncomms2327.

33 X. Yu, J. Joseph and A. Manthiram, *J. Mater. Chem. A*, 2015, **3**, 15683–15691.

34 Y. S. Su and A. Manthiram, *Nat. Commun.*, 2012, **3**, 1–6.

35 M. J. Lacey, A. Yalamanchili, J. Maibach, C. Tengstedt, K. Edström and D. Brandell, *RSC Adv.*, 2016, **6**, 3632–3641.

36 S. S. Zhang, *J. Power Sources*, 2016, **322**, 99–105.

37 A. Jozwiuk, B. B. Berkes, T. Weiß, H. Sommer, J. Janek and T. Brezesinski, *Energy Environ. Sci.*, 2016, **9**, 2603–2608.

38 D. Bresser, S. Passerini and B. Scrosati, *Chem. Commun.*, 2013, **49**, 10545–10562.

39 United States Patent Office, 3043896, 1962.

40 X. Ji, K. T. Lee and L. F. Nazar, *Nat. Mater.*, 2009, **8**, 500–506.

41 C. Cavallo, M. Agostini, J. P. Genders, M. E. Abdelhamid and A. Matic, *J. Power Sources*, 2019, **416**, 111–117.

42 C. K. Chan, H. Peng, G. Liu, K. Mcilwrath, X. F. Zhang, R. A. Huggins and Y. Cui, 2007, 31–35.

43 J. Scheers, S. Fantini and P. Johansson, *J. Power Sources*, 2014, **255**, 204–218.

44 Q. Pang, A. Shyamsunder, B. Narayanan, C. Y. Kwok, L. A. Curtiss and L. F. Nazar, *Nat. Energy*, 2018, **3**, 783–791.

45 Y. Aihara, S. Ito, R. Omoda, T. Yamada, S. Fujiki, T. Watanabe, Y. Park and S. Doo, *Front. Energy Res.*, 2016, **4**, 1–8.

46 T. Yamada, S. Ito, R. Omoda, T. Watanabe, Y. Aihara, M. Agostini, U. Ulissi, J. Hassoun and B. Scrosati, *J. Electrochem. Soc.*, 2015, **162**, A646–A651.

47 J. C. Bachman, S. Muy, A. Grimaud, H. H. Chang, N. Pour, S. F. Lux, O. Paschos, F. Maglia, S. Lupart, P. Lamp, L. Giordano and Y. Shao-Horn, *Chem. Rev.*, 2016, **116**, 140–162.

48 A. Manthiram, X. Yu and S. Wang, *Nat. Rev. Mater.*, 2017, **2**, 1–16.

49 M. Agostini, S. Xiong, A. Matic and J. Hassoun, *Chem. Mater.*, 2015, **27**, 4604–4611.

50 D. H. Lim, M. Agostini, F. Nitze, J. Manuel, J. H. Ahn and A. Matic, *Sci. Rep.*, 2017, **7**, 6327.

51 M. Agostini, D. H. Lim, M. Sadd, J. Y. Hwang, S. Brutti, J. W. Heo, J. H. Ahn, Y. K. Sun and A. Matic, *ChemSusChem*, 2018, **11**, 2981–2986.

52 M. Agostini, D. J. Lee, B. Scrosati, Y. K. Sun and J. Hassoun, *J. Power Sources*, 2014, **265**, 14–19.

53 J. He, G. Hartmann, M. Lee, G. S. Hwang, Y. Chen and A. Manthiram, *Energy Environ. Sci.*, 2019, **12**, 344–350.

54 Q. Pang, D. Kundu and L. F. Nazar, *Mater. Horizons*, 2016, **3**, 130–136.

55 S. H. Chung, L. Luo and A. Manthiram, *ACS Energy Lett.*, 2018, **3**, 568–573.

56 S. H. Chung and A. Manthiram, *Adv. Mater.*, 2018, **30**, 1–9.

57 C. Tan, T. M. M. Heenan, R. F. Ziesche, S. R. Daemi, J. Hack, M. Maier, S. Marathe, C. Rau, D. J. L. Brett and P. R. Shearing, *ACS Appl. Energy Mater.*, 2018, **1**, 5090–5100.

58 J.-T. Yeon, J.-Y. Jang, J.-G. Han, J. Cho, K. T. Lee and N.-S. Choi, *J. Electrochem. Soc.*, 2012, **159**, A1308–A1314.

59 W. Zhu, A. Paolella, C. S. Kim, D. Liu, Z. Feng, C. Gagnon, J. Trottier, A. Vijh, A. Guerfi, A. Mauger, C. M. Julien, M. Armand and K. Zaghib, *Sustain. Energy Fuels*, 2017, **1**, 737–747.

60 S. Waluś, C. Barchasz, J. F. Colin, J. F. Martin, E. Elkaïm, J. C. Leprêtre and F. Alloin, *Chem. Commun.*, 2013, **49**, 7899–7901.

61 J. Hannauer, J. Scheers, J. Fullenwarth, B. Fraisse, L. Stievano and P. Johansson, *ChemPhysChem*, 2015, **16**, 2755–2759.

62 M. Hagen, P. Schiffels, M. Hammer, S. Dörfler, J. Tübke, M. J. Hoffmann, H. Althues and S. Kaskel, *J. Electrochem. Soc.*, 2013, **160**, A1205–A1214.

63 H. L. Wu, L. A. Huff and A. A. Gewirth, *ACS Appl. Mater. Interfaces*, 2015, **7**, 1709–1719.

64 Q. Zou and Y. C. Lu, *J. Phys. Chem. Lett.*, 2016, **7**, 1518–1525.

65 M. U. M. Patel, R. Demir-Cakan, M. Morcrette, J. M. Tarascon, M. Gaberscek and R. Dominko, *ChemSusChem*, 2013, **6**, 1177–1181.

66 N. A. Cañas, D. N. Fronczek, N. Wagner, A. Latz and K. A. Friedrich, *J. Phys. Chem. C*, 2014, **118**, 12106–12114.

67 M. Cuisinier, P. E. Cabelguen, S. Evers, G. He, M. Kolbeck, A. Garsuch, T. Bolin, M. Balasubramanian and L. F. Nazar, *J. Phys. Chem. Lett.*, 2013, **4**, 3227–3232.

68 Q. Wang, J. Zheng, E. Walter, H. Pan, D. Lv, P. Zuo, H. Chen, Z. D. Deng, B. Y. Liaw, X. Yu, X. Yang, J.-G. Zhang, J. Liu and J. Xiao, *J. Electrochem. Soc.*, 2015, **162**, A474–A478.

69 J. Tan, D. Liu, X. Xu and L. Mai, *Nanoscale*, 2017, **9**, 19001–19016.

70 M. Wild, L. O'Neill, T. Zhang, R. Purkayastha, G. Minton, M. Marinescu and G. J. Offer, *Energy Environ. Sci.*, 2015, **8**, 3477–3494.

71 C. V. Raman and K. S. Krishnan, *Nature*, 1928, **121**, 501–502.

72 P. Larkin, *Infrared and Raman Spectroscopy: Principles and Spectral Interpretation*, Elsilvier, Amsterdam, 2011.

73 EL-CELL, ECC-Opto-Std, https://el-cell.com/products/test-cells/optical-test-cells/ecc-opto-std, (accessed 11 October 2019).